WRF-Chem Sensitivity to Vertical Resolution During a Saharan Dust Event

J. C. Teixeira[a,], A. C. Carvalho[b], Paolo Tuccella[c], Gabriele Curci[c], A. Rocha[a]

[a]*Department of Physics, CESAM, University of Aveiro, Campus Universitario de Santiago 3810-193 Aveiro, Portugal*

[b]*CENSE, Departament of Science Environmental Engineering, Faculdade de Ciências e Tecnologia, Universidade Nova de Lisboa, 2829-516 Caparica, Portugal*

[c]*Department of Physical and Chemical Sciences, University of L'Aquila, L'Aquila, Italy*

Abstract

The Saharan dust event that occurred between the 22nd and 30th of June 2012 influenced the atmospheric radiative properties over North Africa, the Iberian Peninsula, the Western Mediterranean basin, extending its effects to France and Southern England. This event is well documented in satellite imagery, as well as on the air quality stations over the Iberian Peninsula and the AERONET NASA network. In order to assess the effect of the model vertical resolution on the extinction coefficient fields, as a proxy to the particulate matter concentrations in the atmosphere, the WRF-Chem model was applied during this period over a mother domain with a resolution of 18 km, covering Europe and North Africa. To this end five model setups differing in the number of vertical levels were tested. Model skills were evaluated by comparing the model results with CALIPSO and EARLINET LIDAR data. Results show that the model is able to simulate the higher level aerosol transport but are susceptible to the vertical resolution used. This is due to the thickness of the transport layers which is, eventually, thinner than the vertical resolution of the model.When comparing model results to the observed vertical profiles, it becomes evident that the broad features of the extinction coefficient profile are generally reproduced in all model configurations, but finer details are captured only by the higher resolution simulations.

Keywords: Dust event, Model Sensitivity, Aerosol, WRF-Chem, Vertical resolution

Email address: jcmt@ua.pt (J. C. Teixeira)

1. Introduction

Over the last years full attention has been given to the modelling of aerosols by the scientific community with a special emphasis on Saharan dust outbreaks (Pey et al., 2013; Bozlaker et al., 2013; Laken et al., 2014).

It is known that dust outbreaks can travel long distances, and that high amounts of dust are transported above the mixing layer at a typical height between four to five kilometres in the free troposphere, often in a thin plume that can grow up to one kilometre thick (Borge et al., 2008; Guerrero-Rascado et al., 2009; Yang et al., 2012), having regional to continental impact on the particulate matter measured in air quality networks and may also affect, directly and indirectly, the atmospheric radiative budget.Moreover, the study of dust outbreaks becomes of high interest as these particles can interact with solar and thermal radiation, perturbing the Earth's radiative budget, with consequent impacts on climate (Santos et al., 2013; Antón et al., 2014) and also changing cloud microphysical properties by acting as cloud condensation nuclei (Weinzierl et al., 2011; Alam et al., 2014). Therefore, the understanding of the sensitivity of modelled simulations to the user defined parameters is crucial in order to get the most of the modelled results.

Using a fully coupled meteorology-chemistry-aerosol model using different aerosol mechanisms Zhao et al. (2010) investigate the modelling sensitivities to dust emissions and aerosol size treatments over North Africa. In their work the authors have shown the differences given by each different mechanism, as well as the effect on the shortwave radiative forcing. More recently, Fast et al. (2014) studied the performance of the Weather Research and Forecasting regional model with chemistry (WRF-Chem) in simulating the spatial and temporal variations in aerosol mass, composition, and size. Albeit showing that the model is capable to reproduce the overall synoptic conditions that controls the transport and mixing of trace gases and aerosols, and hence the overall spatial and temporal variability of aerosols and their precursors, there are cases where the local transport of some aerosol plumes were either too slow or too fast.

The impact of the vertical discretization on model results has been address by several authors and different approaches have been used to tackle it. An example of such approach is the development of a parametrization that allows to take into account the sub-grid dispersion and mixing

(Byun and Dennis, 1995). Yet, the non-linearity of the vertical profile makes this method hard to implement for every atmospheric dynamical setting. Several authors have also approached this problem by coupling the regional scale model with a large eddy simulation models in order to resolve the sub-grid processes that occur (Aristodemou et al., 2009; Hara et al., 2009). However, this technique is difficult to apply over large domains and it is not suitable for long term modelling due to its computational costs. Lastly, by decreasing the vertical grid increments, thus increasing the vertical model resolution, a better discretization can be achieved keeping the physical consistency between the meteorological and chemical variables (Byun and Dennis, 1995; Menut et al., 2013). It is known that physical features that can be well resolved by the horizontal grid increment should also be resolvable by the vertical grid increment (and vice versa). If the vertical grid increment is too coarse to satisfy this criterion, the resulting truncation error will generate spurious gravity waves during the simulation and the features will be poorly rendered by the model (Warner, 2010).

The mathematical relationship that defines consistency between the vertical and horizontal grid increments has been defined differently by different authors. However, the studies found in the literature are often mechanism dependent (Pecnick and Keyser, 1989; Lindzen and Fox-Rabinovitz, 1989; Persson and Warner, 1991). The impact of the vertical resolution at surface on chemistry-transport modelling has been addressed by Menut et al. (2013). The authors show in their work that by increasing the vertical discretization the model was able to better reproduce the surface concentrations.

Southern Europe countries are exposed to the influence of Saharan dust outbreaks (Guerrero-Rascado et al., 2009; Santos et al., 2013). Due to their impacts on air quality several institutions have implemented operational products on atmospheric dust loads (Terradellas et al., 2014). Up to the moment the WRF-chem model has not been implemented in operational mode for this purpose and diagnostic studies are still scarce over the Iberian Peninsula (IP). The objective of the present work lays on the study of the influence of the vertical grid resolution on the dust lift and transport with the WRF-chem model. This is accomplished by using five different vertical model discretizations and comparing the modelled results with LIDAR observations, both from satellite and from surface.

2. Method and Data

2.1. Model Setup

A Saharan dust event that occurred between 22th and 30th of June 2012 has influenced the atmospheric radiative properties over North Africa, the Iberian Peninsula (IP) and the Western Mediterranean basin, extending to France and Southern England. This event is well documented in satellite imagery as well as in the air quality stations over the IP and the AERONET NASA network.

The location of the primary dust sources in North Africa has already been identified by several authors (Prospero et al., 2002; Obregón et al., 2012) and the circulation patterns associated with the dust transport is well documented in the literature (Guerrero-Rascado et al., 2009; Obregón et al., 2012). Taking this knowledge into account a domain covering both the IP and North Africa was designed, as shown in Figure 1, in order to correctly simulate the dust source, the transport and the particulate matter concentration at the air quality locations.

The community model WRF-Chem version 3.5.1 (Grell et al., 2005) was used to simulate all the identified period taking into consideration a 48 hours spin up. Initial and lateral boundary conditions from ERA-Interim reanalysis (Dee et al., 2011) for meteorological fields and MOZART-4/GEOS-5 (Emmons et al., 2010) for chemical species with the Pfister et al. (2011) implementation were provided to the model at six hour intervals. Grided anthropogenic emissions were calculated on the basis of two available emission inventories datasets, namely, the European Monitoring and Evaluation Program (EMEP) data base (`www.ceip.at/emission-data-webdab/emissions-used-in-emep-models`) over Europe complemented with the REanalysis of the TROpospheric chemical composition over the past 40yr RETRO emission inventory. The EMEP inventory for 2011 provided total annual emission of nitrogen oxides (NOx), carbon monoxide (CO), sulphur oxides (SOx), ammonia (NH4), non-methane volatile organic compounds (NMVOC), and particulate matter (PM) over Europe with a grid resolution of 50 km grouped in 11 source types. The procedure followed to build the emissions interface is derived from that of the CHIMERE model (Bessagnet et al., 2008) and adapted by Tuccella et al. (2012) specifically for WRF-Chem. For the model domain not covered by the EMEP emissions, the standard REanalysis of the TRO-

pospheric chemical composition over the past 40yr (RETRO) emission inventory, with a resolution of 50 km, were used following the Freitas et al. (2010) methodology. Fire emissions for the simulated period were taken from the NCAR's Fire Inventory (FINN) emissions model and given to the model according to the Wiedinmyer et al. (2011) procedure. The biogenic emissions are calculated through the MEGAN Model (Model of Emissions of Gases and Aerosols from Nature) (Guenther et al., 2006).

The gas phase chemical mechanism used in this work was the CBMZ (Carbon Bond Mechanism) photochemical mechanism (Zaveri and Peters, 1999) and the aerosol mechanism the MOSAIC (Model for Simulating Aerosol Interactions and Chemistry) aerosol model considering eight sectional aerosol bins (Zaveri et al., 2008) implemented by Fast et al. (2006) into WRF-Chem, which also includes more complex treatments of aerosol radiative properties and photolysis rates.

The set of parametrizations used in the model physical configuration were the Lin et al. microphysics Scheme (Lin et al., 1983), Goddard shortwave radiation scheme (Chou and Suarez, 1994), RRTMG (Rapid Radiative Transfer Model) longwave radiation model (Mlawer et al., 1997), the MM5 similarity surface layer scheme (Zhang and Anthes, 1982), the Noah Land Surface Model (Tewari et al., 2004), the MellorYamadaJanjic Planetary Boundary Layer scheme (Janjic, 1994) and the Grell 3D Ensemble Scheme for cumulus parametrization (Grell and Dévényi, 2002). The main chemical parametrization used were the Fast-J photolysis scheme (Wild et al., 2000), GOCART with AFWA modifications described by Ginoux et al. (2001) was used to include dust and sea salt emissions. The Wesely (1989) dry deposition velocities parametrization are used, as well as, the full wet deposition module, coupled with aqueous chemistry, available in WRF/Chem, and aerosols direct and indirect effects are accounted in the simulations (Chapman et al., 2009). A detailed description of the WRF-Chem model and the computation of aerosol optical properties can be found in Fast et al. (2006) and Barnard et al. (2010).

To study the influence of the vertical grid resolution on the dust lift and transport four simulations were performed using different numbers of vertical level, starting at 30 and going up to 100 vertical levels - 030L, 040L, 060L, 080L and 100L. All these simulations have an horizontal resolution of 18 km and an adaptative time step always lower than 108 seconds was applied to

ensure numerical stability.

2.2. Observed Data

To assess the model skill in simulating the vertical distribution of aerosols two observed dataset were used. The first dataset consists on the 532 nm extinction coefficient from Cloud-Aerosol Lidar Infrared Pathfinder Satellite Observations (CALIPSO) Level 2 Aerosols Profile product derived from the CALIOP backscatter LIDAR instrument. This product also accounts for the retrieval uncertainties derived in 5 km along-track segments at 60 m vertical resolution, separated into contiguous daytime and night time granule files and the extinction coefficient is derived using the Hybrid Extinction Retrieval Algorithm described by Young and Vaughan (2009). The night and day time satellite passages as well as all the available passages matching the domain of interest and period were considered - Figure 1.

The second dataset corresponds to the 532 nm extinction coefficients for the ground LIDAR stations of the European Aerosol Research LIdar NETwork (EARLINET). A full description of this dataset can be found in the Schneider et al. (2000) report. From this network three stations located inside the domain of interest were considered - Évora, Madrid and Barcelona. The location of these stations can be found in Figure 1.

2.3. Model Skill Analysis

Several measures, based on Keyser and Anthes (1977) and Pielke (2002), were used to quantify the model skill,namely:

- Accuracy, as the degree of closeness of measurements of a quantity to that quantity actual value.

- Deviation of the modelled data in relation to observed values:

$$\phi_i' = \phi_i - \phi_{i,obs} \tag{1}$$

- Bias, which represents the mean deviation of the modelled data in relation to the observed values.

$$Bias = \frac{1}{N}\sum_{i=1}^{N}\phi_i' \tag{2}$$

- The Root Mean Square Error.

$$E = \sqrt{\frac{\sum_{i=1}^{N}\left(\phi_i - \phi_{i,obs}\right)^2}{N}} \tag{3}$$

- The Root Mean Square Error after the removal of a constant bias.

$$E_{UB} = \sqrt{\frac{\sum_{i=1}^{n}\left[\left(\phi_i - \overline{\phi}\right) - \left(\phi_{i,obs} - \overline{\phi_{obs}}\right)\right]^2}{N}} \tag{4}$$

- Standard deviation for the modelled - equation 5 - and observed - equation 6 - data.

$$S = \sqrt{\frac{\sum_{i=1}^{n}\left(\phi_i - \overline{\phi}\right)^2}{N}} \tag{5}$$

$$S_{obs} = \sqrt{\frac{\sum_{i=1}^{n}\left(\phi_{i,obs} - \overline{\phi_{obs}}\right)^2}{N}} \tag{6}$$

were i is the temporal index and N is the number of elements of ϕ considered.

Given this, a perfect forecast would observe the following criteria:

- $S \approx S_{obs}$
- $E < S_{obs}$
- $E_{UB} < S_{obs}$

- $Bias^2 < E^2$
- Pearson Correlation (R) ≈ 1

Furthermore, the modelled results are considered to be accurate when:
$\phi_{i,obs} - \Delta\phi_{i,obs} < \phi_i < \phi_{i,obs} + \Delta\phi_{i,obs}$.

3. Results and Discussion

3.1. Synoptic Setting

During the first three days of the simulated period - 23rd to 25th of June - the IP is under the influence of an anticyclonic system that prevents the arrival of the frontal system that is developing in the North Atlantic. This blockage produces clear sky weather conditions and a strong surface heating, leading to the development of thermal low over the IP. At the same time, a deep convective storm initiates and matures over North Africa. This storm produces strong surface winds that lift high amounts of dust, creating an atmospheric mixing layer with high dust loads. This event is well documented in satellite imagery, in the data acquired at the air quality stations over the IP and the AERONET NASA network (not shown but analysed).

At the following days the high pressure system undergoes a northward displacement, allowing the dust rich air mass transport to the North, reaching the southern and western coast of the IP on the 26th of June. During this event the IP is free of clouds, the air mass that is transported from North Africa creates a fairly dry environment and the aerosol dust mass transported to the study domain is not polluted, therefore, hygroscopicity and aerosol indirect effects are not expected to play a dominant role.

In the end of the simulated period - 28th to 30th of June - a frontal system sweeps the study area, bringing cold and dust free air to the IP.

According to MODIS satellite images few fire hot spots were sensed over the IP during the simulated period of this event (not shown) making this event an opportunity to study the influence of dust aerosol in the atmosphere during summer time, excluding the influence of major wildfires usually occurring over the IP during this season.

3.2. CALIPSO vs WRF Model

The WRF-Chem simulated extinction coefficient at 532 nm for three CALIPSO satellite swaths on 26 and 28 of June at 0200 UTC has well as on the 28th of June at 1300 UTC was interpolated to match the CALIPSO track and compared with CALIPSO retrieved extinction coefficient at 532 nm for the five performed simulations, as can be observed in Figure 2.

As can be seen in Figure 2, WRF-Chem overestimates the extinction coefficient retrieved by CALIPSO but captures the temporal and vertical variations along the CALIPSO track. Moreover, all the simulations are capable to broadly reproduce the CALIPSO pattern. However, a finer discretization of the model vertical grid produces differences to the modelled extinction coefficient, specially along the border of high values of extinction coefficient, in areas where high gradients are present or where local and small scale processes are dominant. For all the compared days, it can be observed that the increase of vertical resolution produces extinction coefficient patterns that do not reach as high as the lower resolution simulations. Moreover, it can be seen that for areas with high spatial variability of this optical property - e.g. 28th of June at 0200 UTC around 28 $^{\circ}N$ - and also in areas where the mixing layer processes are dominant in relation to the distribution of aerosols - over 40 $^{\circ}N$ and near the Gibraltar straight (approximated location at 36 N - 5.5 W) - significant differences between simulations can be detected, specially near the surface levels, with the lower resolution simulations showing a more smoothed distribution of the extinction coefficient values and hence of the aerosols loads in the atmosphere.

When comparing the accuracy of the simulations in reproducing the CALIPSO LIDAR extinction coefficient, (table 1), no evident pattern can be recognized. In some cases the increase of the vertical resolution leads to an improvement in the accuracy and in other cases it decreases it. However, all simulations present similar relative accuracy. Nonetheless, it is noteworthy that for the 28th of June at 0200 UTC, the day with more observed grid points, the satellite swath where more small scale features are depicted in the observations, the increase of the vertical resolution produces better results, with the highest accuracy being achieved by the 080L simulation.

By providing an high resolution vertical profile of the extinction coefficient for the study domain, this dataset allows for a unique approach for comparing modelled results with observations.

Table 1: Simulations extinction coefficient accurate grid points (%) in June 2012 - night passages in light grey and day passages in dark grey.

Date \ levels	030L	040L	060L	080L	100L
26 at 0200 UTC	34.3	32.8	31.3	30.9	30.4
26 at 1300 UTC	14.8	17.5	16.1	14.2	16.1
28 at 0200 UTC	17.7	16.2	15.5	20.1	18.4
28 at 1300 UTC	26.5	26.6	24.6	25.7	21.1
30 at 0200 UTC	37.8	37.6	35.8	34.1	37.1

However, the acquired observed values are affected by a large uncertainty which is typically $\approx 40\%$ for the extinction coefficient according to Vaughan et al. (2004) and Liu et al. (2008). Moreover, there is often missing data in areas of extreme interest - the lower levels and in areas where important processes are responsible for dust emissions and its distribution in the atmosphere - e.g. for 26th at 0200 UTC and 28th at 1300 UTC. Therefore, the choice of the best simulation considering only this dataset is not straightforward and other data sources must be considered.

3.3. EARLINET vs WRF Model

The EARLINET LIDAR extinction coefficient vertical profiles give an estimate of the aerosol distribution and evolution during the Saharan dust event in the lower troposphere - between 500 and 3000 m of altitude - providing a best estimate of aerosol in these levels when compared to the CALIPSO products. The combination of this dataset with the CALIPSO allows us to obtain a better estimate of the model skill and permit to a better understanding of the effect of the vertical discretization on the model results.

Figure 3 shows the skill measures for all the performed simulations, using all stations within the domain with available data during the study period. In this figure it is possible to see that all simulations overestimate the observed variability - $S/S_{obs} > 1$ - as well as the observed extinction coefficient - $E/S_{obs} > 0$ - even after the removal of a constant bias ($E_{UB}/S_{obs} > 0$). However, the $BIAS^2/E^2$ is small (close to zero), showing that the error associated with the peak displacement of

the model results is small when compared to the its E. Moreover, the majority of the simulations present a Pearson Correlation (R) near 50 %. These results of skill measures also show an increase of skill for the simulations with higher resolutions, with the exception of the simulation 100L, where the skill measure shows a deterioration.

The simulation that performed best when considering this skill analysis was the 080L. This result can be associated with a better description of the local scale processes that dominate over areas that significantly affect the dust transport. Namely near Gibraltar where the Levant wind (gap wind) together with land-ocean-land discontinuity will create a blockage to the dust transport within the mixing layer. Changing the vertical resolution will therefore change the vertical distribution of dust. It should be stressed that during the simulated period the atmosphere is dry (air mass from North Africa) and there is no moist convection nor other phenomena that could significantly change the aerosol distribution.

The deterioration of skill when increasing the resolution from 80 to 100 levels may happen due to limitation in numerics, i.e. WRF-Chem diffusion is explicitly determined. Moreover the increase of vertical resolution is not followed by an increase of the horizontal resolution, leading to poorly rendered features, which is an expected result. Also with this resolution the model can implicitly solve some features which are also being parametrized. Nonetheless, the skill of the 100L simulation is higher than the skill of simulations that use vertical levels commonly used (30 to 40 levels).

The previous analysis allows for the quantification of the model skill when compared to observations. In cases where the model is capable of reproducing the observed pattern, but with different amplitude or displacement, it can be considered that the model does not have skill in reproducing the observations.

The vertical profiles of extinction coefficient at 532 nm for Barcelona for several of the simulated days can be seen in Figure 4. This figure illustrates the aforementioned effect in Figure 4 a) the model is able to reproduce accurately the spacial location of the layer where high concentration of aerosols are present - high extinction coefficient - in all simulations, but is failing to reproduce their amount. Similarly, in Figure 4 d) the same effect occurs but in this case, the change of the

vertical levels significantly affects the location of the aerosol layer.

In Figure 4 b) two distinct aerosol layers can be identified at an altitude of 1.0 and 2.5 km - through the high extinction coefficient values. In this case the model simulates the first layer above its observed location and also underestimates its extinction coefficient magnitude; it is noticeable that the number of levels for the vertical resolution choice produces different aerosol amounts- the higher the resolution the higher the extinction coefficient. Moreover, it can be seen that the model presents lack of skill in simulating the second aerosol layer. Only the 60 level simulation was able to capture a weak signal in simulating this layer.

In the case shown in Figure 4 c) it is possible to see that the model has skill in simulating the extinction coefficient profile and it is able to reproduce the observed profile in every performed simulation with few differences on the location of the aerosols layers.

The simulation $BIAS$ considering the observed period and all EALINET stations can be seen in table 2

Table 2: Simulations BIAS for the extinction coefficient profile (km^{-1}) - all EARLINET stations available for the study domain were used.

levels	030L	040L	060L	080L	100L
$BIAS$	0.029	0.027	0.025	0.016	0.022

Considering the previous analysis it is possible to see that the the different simulations produce significant changes to the $BIAS$. From table 2 it is possible to see that by increasing the vertical resolution to 80 vertical levels, there is a reduction in model $BIAS$, and a consequent decrease in the extinction coefficient of 45 %.

As mentioned before, Zhao et al. (2010) investigate the modelling sensitivities to dust emissions and aerosol size treatments over North Africa. In their work the authors show that the differences given by each different mechanism can lead to an increase of the extinction coefficient as large as 12 % (MADE/SORGRAM compared to MOSAIC). Moreover, the choice of the physical parametrization, (Misenis and Zhang, 2010), and the description of the dust fluxes, (Kang et al., 2011) can significantly change particle matter concentration, especially within the planetary boundary layer.

This analysis of the WRF-Chem simulations and their comparison with the available observations emphasis the importance of the choice of the number of vertical levels when simulating the transport of dust in the atmosphere. The changes to the modelled extinction coefficient depicted in this analysis can be as important as the choice of the model parametrization, providing an overview on the influence of vertical levels in model uncertainties.

4. Concluding Remarks

Atmospheric chemistry models are known to be sensitive to user defined model parameters. This work focuses on the study of the influence of the vertical grid resolution on the dust lift and transport. In order to achieve this goal, a Saharan dust event that occurred between 22th and 30th of June, 2012 was simulated using the WRF-Chem model. Five simulations using different number of vertical levels, 30, 40, 60, 80 and 100 levels, were performed and the results compared against the extinction coefficient LIDAR vertical profile observations, both from CALIPSO satellite and from surface EARLINET stations.

The analysed results have shown that the performed simulations where able to broadly reproduced the temporal and vertical extinction coefficient patterns found in the CALIPSO LIDAR observations. Moreover, it was found that the increase of model vertical resolution better depicts the small scale extinction coefficient patterns that are often associated to regions where local and small scale processes are dominant, and areas of high concentration gradients of aerosols. However, we noticed that increasing the vertical resolution beyond a certain point (from 80 to 100 levels, in our case) may result in no further improvement (or slight deterioration) of model skill. In addition, when comparing the modelled to the EARLINET ground stations, it was possible to observe that the model is able to capture the location of the aerosol layers, but with a large error of its extinction coefficient. The analysis of the skill measures showed that each simulation presented a large error ($E/S_{obs} > 0$) and an overestimation of the observed variability ($S/S_{obs} > 1$). Furthermore, it was also seen that the model is sensitive to the choice of the vertical resolution, showing significant differences in the aerosol layer location and extinction coefficient amplitude as the vertical grid increments are changed. It also shows an increase of the model skill when the vertical resolution

increases, with the best results being achieved for the 080L simulation.

5. Acknowledgements

This work was funded by FEDER funds, through the operational program COMPETE and by national funds, through the National Foundation for Science and Technology (FCT), in the framework of the project CLICURB (EXCL/AAG-MAA/0383/2012). P. Tuccella and G. Curci were supported by the Italian Space Agency in the frame of PRIMES project (contract n. I/017/11/0).

6. References

Alam, K., Trautmann, T., Blaschke, T., Subhan, F., 2014. Changes in aerosol optical properties due to dust storms in the middle east and southwest asia. Remote Sensing of Environment 143, 216–227.

Antón, M., Valenzuela, A., Mateos, D., Alados, I., Foyo-Moreno, I., Olmo, F., Alados-Arboledas, L., 2014. Longwave aerosol radiative effects during an extreme desert dust event in southeastern spain. Atmospheric Research.

Aristodemou, E., Bentham, T., Pain, C., Colvile, R., Robins, A., ApSimon, H., 2009. A comparison of mesh-adaptive les with wind tunnel data for flow past buildings: Mean flows and velocity fluctuations. Atmospheric Environment 43 (39), 6238–6253.

Barnard, J. C., Fast, J. D., Paredes-Miranda, G., Arnott, W., Laskin, A., 2010. Technical note: Evaluation of the wrf-chem" aerosol chemical to aerosol optical properties" module using data from the milagro campaign. Atmospheric Chemistry and Physics 10 (15), 7325–7340.

Bessagnet, B., Menut, L., Curci, G., Hodzic, A., Guillaume, B., Liousse, C., Moukhtar, S., Pun, B., Seigneur, C., Schulz, M., 2008. Regional modeling of carbonaceous aerosols over europefocus on secondary organic aerosols. Journal of Atmospheric Chemistry 61 (3), 175–202.

328 Borge, R., Alexandrov, V., José del Vas, J., Lumbreras, J., Rodríguez, E., 2008. A comprehensive
329 sensitivity analysis of the wrf model for air quality applications over the iberian peninsula.
330 Atmospheric Environment 42 (37), 8560–8574.

331 Bozlaker, A., Prospero, J. M., Fraser, M. P., Chellam, S., 2013. Quantifying the contribution of
332 long-range saharan dust transport on particulate matter concentrations in houston, texas, using
333 detailed elemental analysis. Environmental science & technology 47 (18), 10179–10187.

334 Byun, D. W., Dennis, R., 1995. Design artifacts in eulerian air quality models: Evaluation of
335 the effects of layer thickness and vertical profile correction on surface ozone concentrations.
336 Atmospheric Environment 29 (1), 105–126.

337 Chapman, E. G., Gustafson Jr, W., Easter, R. C., Barnard, J. C., Ghan, S. J., Pekour, M. S., Fast,
338 J. D., 2009. Coupling aerosol-cloud-radiative processes in the wrf-chem model: Investigating the
339 radiative impact of elevated point sources. Atmospheric Chemistry and Physics 9 (3), 945–964.

340 Chou, M.-D., Suarez, M. J., 1994. An efficient thermal infrared radiation parameterization for use
341 in general circulation models. NASA Tech. Memo 104606 (3), 85.

342 Dee, D., Uppala, S., Simmons, A., Berrisford, P., Poli, P., Kobayashi, S., Andrae, U., Balmaseda,
343 M., Balsamo, G., Bauer, P., et al., 2011. The era-interim reanalysis: Configuration and perfor-
344 mance of the data assimilation system. Quarterly Journal of the Royal Meteorological Society
345 137 (656), 553–597.

346 Emmons, L., Walters, S., Hess, P., Lamarque, J.-F., Pfister, G., Fillmore, D., Granier, C., Guen-
347 ther, A., Kinnison, D., Laepple, T., et al., 2010. Description and evaluation of the model for
348 ozone and related chemical tracers, version 4 (mozart-4). Geoscientific Model Development 3 (1),
349 43–67.

350 Fast, J., Allan, J., Bahreini, R., Craven, J., Emmons, L., Ferrare, R., Hayes, P., Hodzic, A., Hol-
351 loway, J., Hostetler, C., et al., 2014. Modeling regional aerosol and aerosol precursor variability

over california and its sensitivity to emissions and long-range transport during the 2010 calnex and cares campaigns. Atmospheric Chemistry and Physics 14 (18), 10013–10060.

Fast, J., Gustafson Jr, W., Easter, R., Zaveri, R., Barnard, J., Chapman, E., Grell, G., 2006. Evolution of ozone, particulates, and aerosol direct forcing in an urban area using a new fully-coupled meteorology, chemistry, and aerosol model. J. Geophys. Res 111 (5), D21305.

Freitas, S., Longo, K., Alonso, M., Pirre, M., Marecal, V., Grell, G., Stockler, R., Mello, R., Sánchez Gácita, M., 2010. A pre-processor of trace gases and aerosols emission fields for regional and global atmospheric chemistry models. Geoscientific Model Development Discussions 3 (2), 855–888.

Ginoux, P., Chin, M., Tegen, I., Prospero, J. M., Holben, B., Dubovik, O., Lin, S.-J., 2001. Sources and distributions of dust aerosols simulated with the gocart model. Journal of Geophysical Research: Atmospheres (1984–2012) 106 (D17), 20255–20273.

Grell, G. A., Dévényi, D., 2002. A generalized approach to parameterizing convection combining ensemble and data assimilation techniques. Geophysical Research Letters 29 (14), 38–1.

Grell, G. A., Peckham, S. E., Schmitz, R., McKeen, S. A., Frost, G., Skamarock, W. C., Eder, B., 2005. Fully coupled online chemistry within the wrf model. Atmospheric Environment 39 (37), 6957–6975.

Guenther, A., Karl, T., Harley, P., Wiedinmyer, C., Palmer, P., Geron, C., et al., 2006. Estimates of global terrestrial isoprene emissions using megan (model of emissions of gases and aerosols from nature). Atmospheric Chemistry and Physics 6 (11), 3181–3210.

Guerrero-Rascado, J. L., Olmo, F., Avilés-Rodríguez, I., Navas-Guzmán, F., Pérez-Ramírez, D., Lyamani, H., Alados-Arboledas, L., 2009. Extreme saharan dust event over the southern iberian peninsula in september 2007: active and passive remote sensing from surface and satellite. Atmos. Chem. Phys 9 (21), 8453–8469.

376 Hara, T., Trini Castelli, S., Ohba, R., Tremback, C., 2009. Validation studies of turbulence closure
377 schemes for high resolutions in mesoscale meteorological models–a case of gas dispersion at the
378 local scale. Atmospheric Environment 43 (24), 3745–3753.

379 Janjic, Z. I., 1994. The step-mountain eta coordinate model: Further developments of the con-
380 vection, viscous sublayer, and turbulence closure schemes. Monthly Weather Review 122 (5),
381 927–945.

382 Kang, J.-Y., Yoon, S.-C., Shao, Y., Kim, S.-W., 2011. Comparison of vertical dust flux by im-
383 plementing three dust emission schemes in wrf/chem. Journal of Geophysical Research: Atmo-
384 spheres (1984–2012) 116 (D9).

385 Keyser, D., Anthes, R. A., 1977. The applicability of a mixed-layer model of the planetary boundary
386 layer to real-data forecasting. Mon. Weather Rev. 105, 1351–1371.

387 Laken, B. A., Parviainen, H., Pallé, E., Shahbaz, T., 2014. Saharan mineral dust outbreaks ob-
388 served over the north atlantic island of la palma in summertime between 1984 and 2012. Quar-
389 terly Journal of the Royal Meteorological Society 140 (680), 1058–1068.

390 Lin, Y.-L., Farley, R. D., Orville, H. D., 1983. Bulk parameterization of the snow field in a cloud
391 model. Journal of Climate and Applied Meteorology 22 (6), 1065–1092.

392 Lindzen, R. S., Fox-Rabinovitz, M., 1989. Consistent vertical and horizontal resolution. Monthly
393 Weather Review 117 (11), 2575–2583.

394 Liu, Z., Omar, A., Vaughan, M., Hair, J., Kittaka, C., Hu, Y., Powell, K., Trepte, C., Winker, D.,
395 Hostetler, C., et al., 2008. Calipso lidar observations of the optical properties of saharan dust: A
396 case study of long-range transport. Journal of Geophysical Research: Atmospheres (1984–2012)
397 113 (D7).

398 Menut, L., Bessagnet, B., Colette, A., Khvorostiyanov, D., 2013. On the impact of the vertical
399 resolution on chemistry-transport modelling. Atmospheric Environment 67, 370–384.

Misenis, C., Zhang, Y., 2010. An examination of sensitivity of wrf/chem predictions to physical parameterizations, horizontal grid spacing, and nesting options. Atmospheric Research 97 (3), 315–334.

Mlawer, E. J., Taubman, S. J., Brown, P. D., Iacono, M. J., Clough, S. A., 1997. Radiative transfer for inhomogeneous atmospheres: Rrtm, a validated correlated-k model for the longwave. Journal of Geophysical Research: Atmospheres (1984–2012) 102 (D14), 16663–16682.

Obregón, M., Pereira, S., Wagner, F., Serrano, A., Cancillo, M., Silva, A., 2012. Regional differences of column aerosol parameters in western iberian peninsula. Atmospheric Environment 62, 208–219.

Pecnick, M., Keyser, D., 1989. The effect of spatial resolution on the simulation of upper-tropospheric frontogenesis using a sigma-coordinate primitive equation model. Meteorology and Atmospheric Physics 40 (4), 137–149.

Persson, P. O. G., Warner, T. T., 1991. Model generation of spurious gravity waves due to inconsistency of the vertical and horizontal resolution. Monthly weather review 119 (4), 917–935.

Pey, J., Querol, X., Alastuey, A., Forastiere, F., Stafoggia, M., 2013. African dust outbreaks over the mediterranean basin during 2001–2011: Pm 10 concentrations, phenomenology and trends, and its relation with synoptic and mesoscale meteorology. Atmospheric Chemistry and Physics 13 (3), 1395–1410.

Pfister, G., Parrish, D., Worden, H., Emmons, L., Edwards, D., Wiedinmyer, C., Diskin, G., Huey, G., Oltmans, S., Thouret, V., et al., 2011. Characterizing summertime chemical boundary conditions for airmasses entering the us west coast. Atmospheric Chemistry and Physics 11 (4), 1769–1790.

Pielke, R., 2002. Mesoscale meteorological modeling. Vol. 78. Academic Pr.

Prospero, J. M., Ginoux, P., Torres, O., Nicholson, S. E., Gill, T. E., 2002. Environmental characterization of global sources of atmospheric soil dust identified with the nimbus 7 total ozone mapping spectrometer (toms) absorbing aerosol product. Reviews of geophysics 40 (1), 2–1.

Santos, D., Costa, M. J., Silva, A. M., Salgado, R., 2013. Modeling saharan desert dust radiative effects on clouds. Atmospheric Research 127, 178–194.

Schneider, J., Balis, D., Böckmann, C., Bösenberg, J., Calpini, B., Chaikovsky, A., Comeron, A., Flamant, P., Freudenthaler, V., Hågård, A., et al., 2000. A european aerosol research lidar network to establish an aerosol climatology (earlinet). Journal of aerosol science 31, 592–593.

Terradellas, E., Basart, S., Baldasano, J. M., 10 2014. Evaluation of multi-model dust forecasts. Tech. rep., Regional Center For Northern Africa, Middle East And Europe Of The WMO SDS-WAS.

Tewari, M., Chen, F., Wang, W., Dudhia, J., LeMone, M., Mitchell, K., Ek, M., Gayno, G., Wegiel, J., Cuenca, R., 2004. Implementation and verification of the unified noah land surface model in the wrf model. In: 20th conference on weather analysis and forecasting/16th conference on numerical weather prediction. pp. 11–15.

Tuccella, P., Curci, G., Visconti, G., Bessagnet, B., Menut, L., Park, R. J., 2012. Modeling of gas and aerosol with wrf/chem over europe: Evaluation and sensitivity study. Journal of Geophysical Research: Atmospheres (1984–2012) 117 (D3).

Vaughan, M. A., Young, S. A., Winker, D. M., Powell, K. A., Omar, A. H., Liu, Z., Hu, Y., Hostetler, C. A., 2004. Fully automated analysis of space-based lidar data: An overview of the calipso retrieval algorithms and data products. In: Remote Sensing. International Society for Optics and Photonics, pp. 16–30.

Warner, T. T., 2010. Numerical weather and climate prediction. Cambridge University Press.

Weinzierl, B., Sauer, D., Esselborn, M., Petzold, A., Veira, A., Rose, M., Mund, S., Wirth, M., Ansmann, A., Tesche, M., et al., 2011. Microphysical and optical properties of dust and tropical

biomass burning aerosol layers in the cape verde regionan overview of the airborne in situ and lidar measurements during samum-2. Tellus B 63 (4), 589–618.

Wesely, M., 1989. Parameterization of surface resistances to gaseous dry deposition in regional-scale numerical models. Atmospheric Environment (1967) 23 (6), 1293–1304.

Wiedinmyer, C., Akagi, S., Yokelson, R. J., Emmons, L., Al-Saadi, J., Orlando, J., Soja, A., 2011. The fire inventory from ncar (finn): A high resolution global model to estimate the emissions from open burning. Geoscientific Model Development 4, 625.

Wild, O., Zhu, X., Prather, M. J., 2000. Fast-j: Accurate simulation of in-and below-cloud photolysis in tropospheric chemical models. Journal of Atmospheric Chemistry 37 (3), 245–282.

Yang, W., Marshak, A., Várnai, T., Kalashnikova, O. V., Kostinski, A. B., 2012. Calipso observations of transatlantic dust: vertical stratification and effect of clouds. Atmospheric Chemistry and Physics 12 (23), 11339–11354.

Young, S. A., Vaughan, M. A., 2009. The retrieval of profiles of particulate extinction from cloud-aerosol lidar infrared pathfinder satellite observations (calipso) data: Algorithm description. Journal of Atmospheric and Oceanic Technology 26 (6), 1105–1119.

Zaveri, R. A., Easter, R. C., Fast, J. D., Peters, L. K., 2008. Model for simulating aerosol interactions and chemistry (mosaic). Journal of Geophysical Research: Atmospheres (1984–2012) 113 (D13).

Zaveri, R. A., Peters, L. K., 1999. A new lumped structure photochemical mechanism for large-scale applications. Journal of Geophysical Research: Atmospheres (1984–2012) 104 (D23), 30387–30415.

Zhang, D., Anthes, R. A., 1982. A high-resolution model of the planetary boundary layer-sensitivity tests and comparisons with sesame-79 data. Journal of Applied Meteorology 21 (11), 1594–1609.

Zhao, C., Liu, X., Leung, L., Johnson, B., McFarlane, S. A., Gustafson Jr, W., Fast, J. D., Easter, R., 2010. The spatial distribution of mineral dust and its shortwave radiative forcing over north africa: modeling sensitivities to dust emissions and aerosol size treatments. Atmospheric Chemistry and Physics 10 (18), 8821–8838.

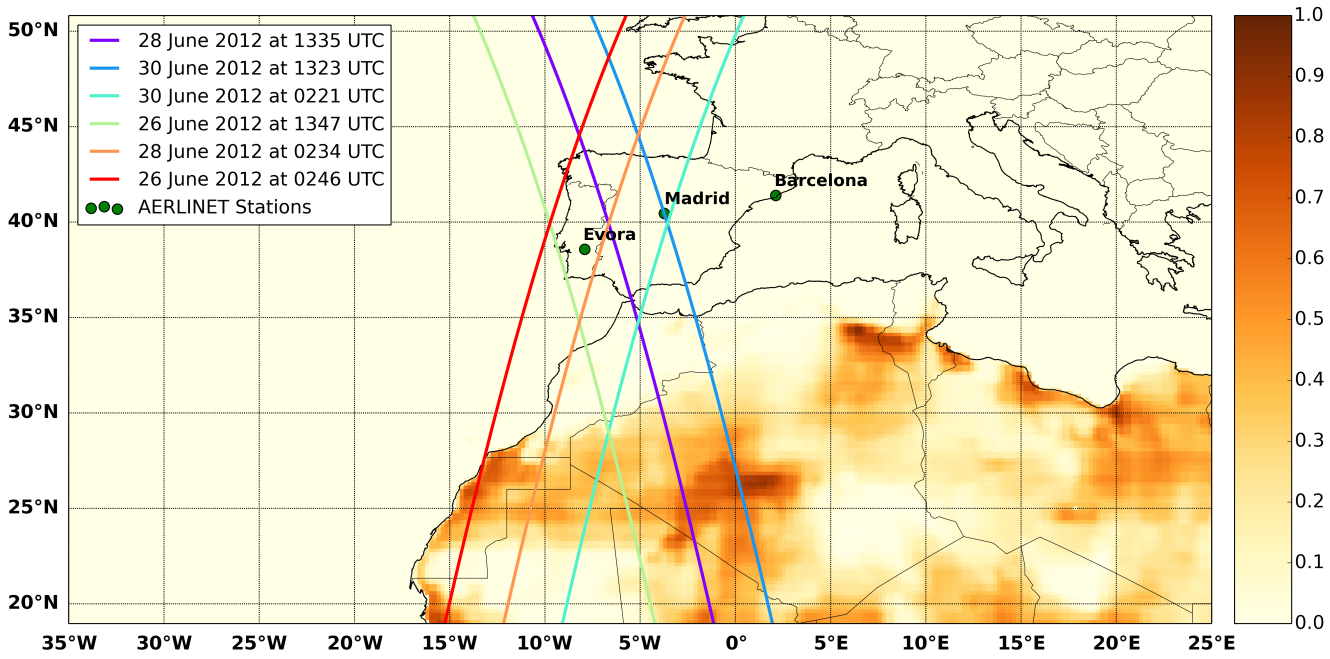

Figure 1: Representation of the model domain, CALIPSO satellite swaths (coloured lines), location of the EARLINET ground stations (green dots) and model surface erodible fraction (shaded).

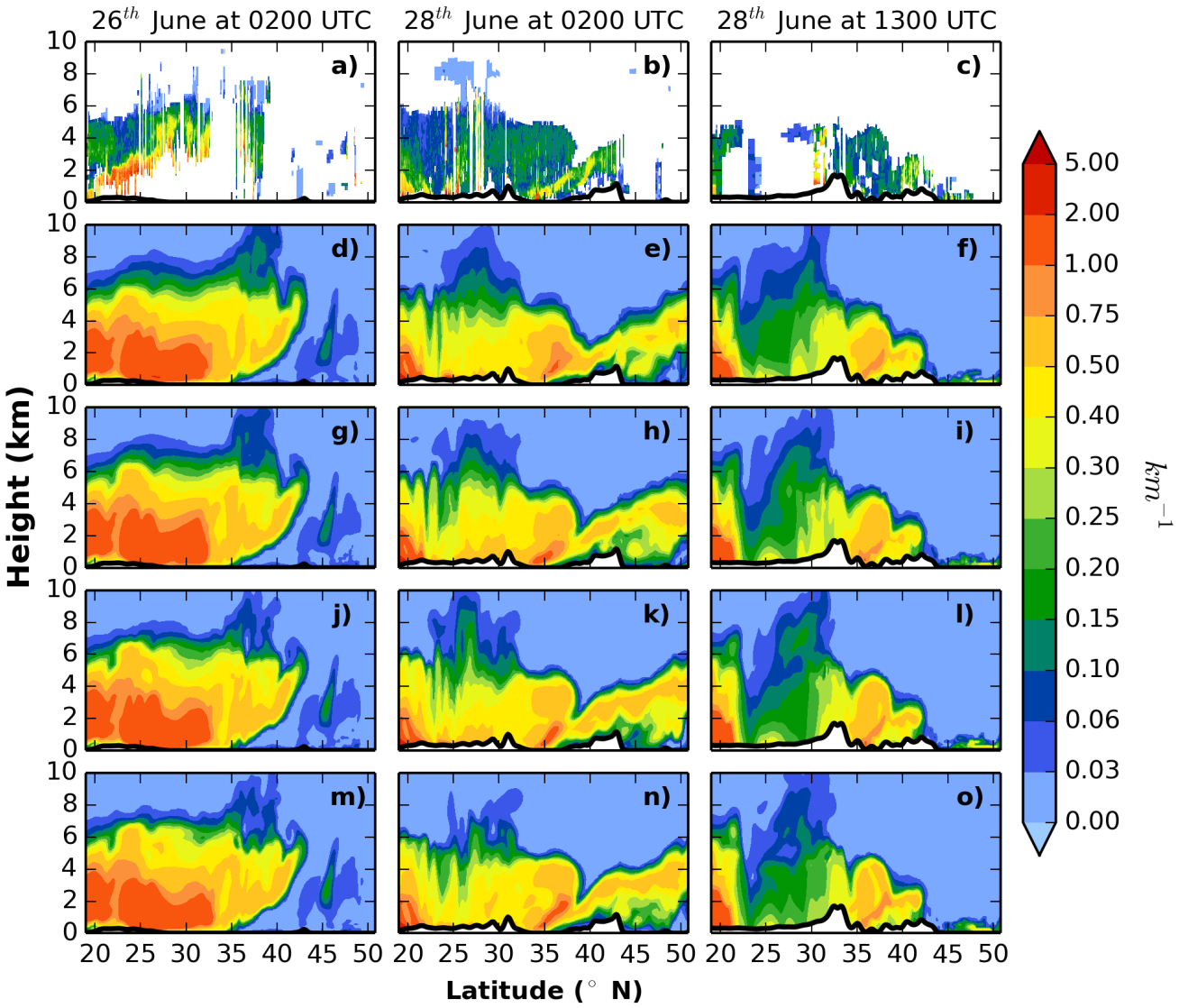

Figure 2: CALIPSO retrieved extinction coefficient (km^{-1}) at 532 nm. The three columns denote the extinction coefficient cross sections on 26th of June at 0200 UTC, 28th of June at 0200 UTC and 28th of June at 1300 UTC. The rows denote, from top to bottom: CALIPSO retrievals, WRF-Chem 030L, 040L, 060L and 080L.

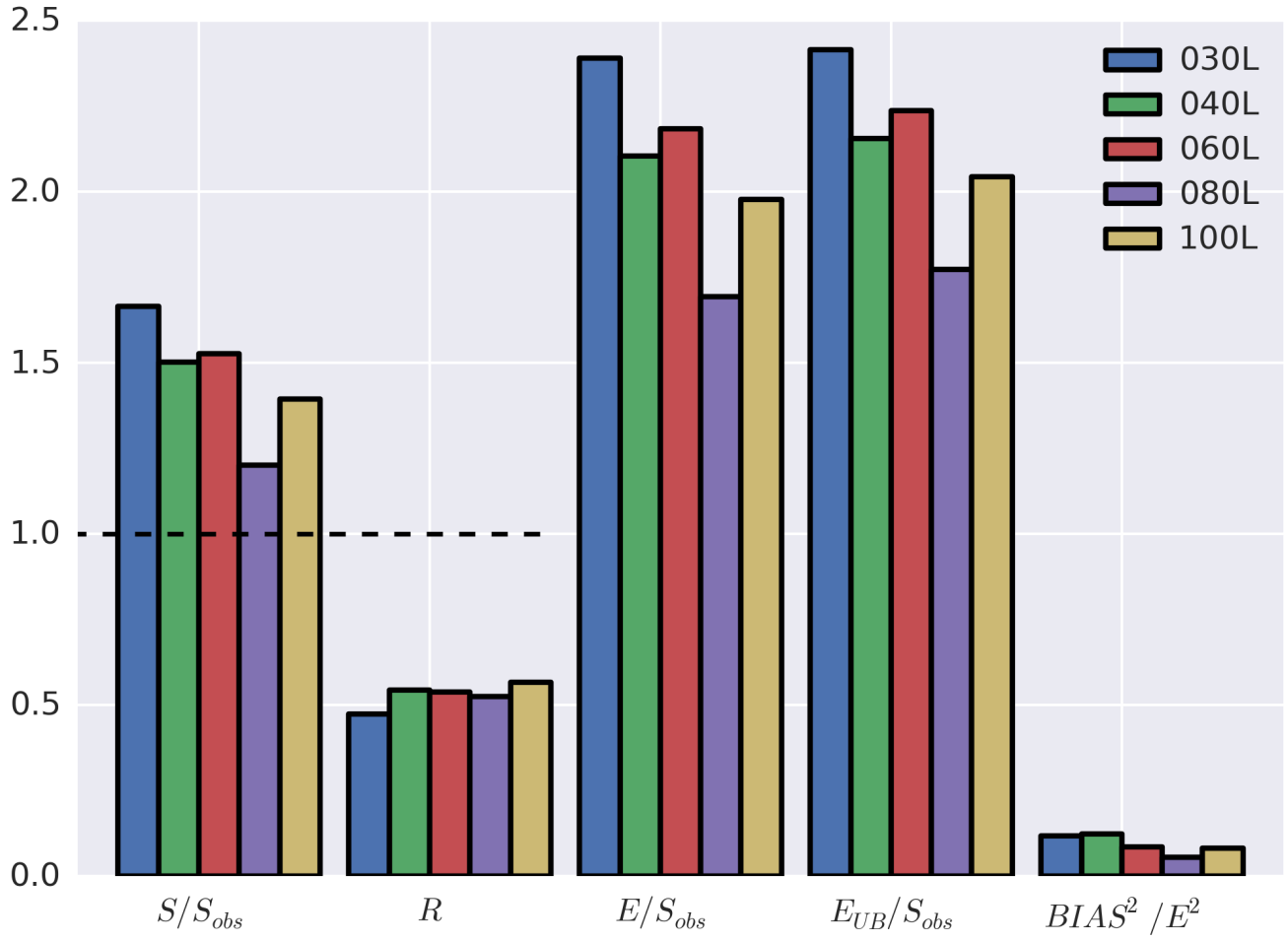

Figure 3: Vertical profiles of extinction coefficient at 532 nm skill chart - all EARLINET stations available for the study domain were used.

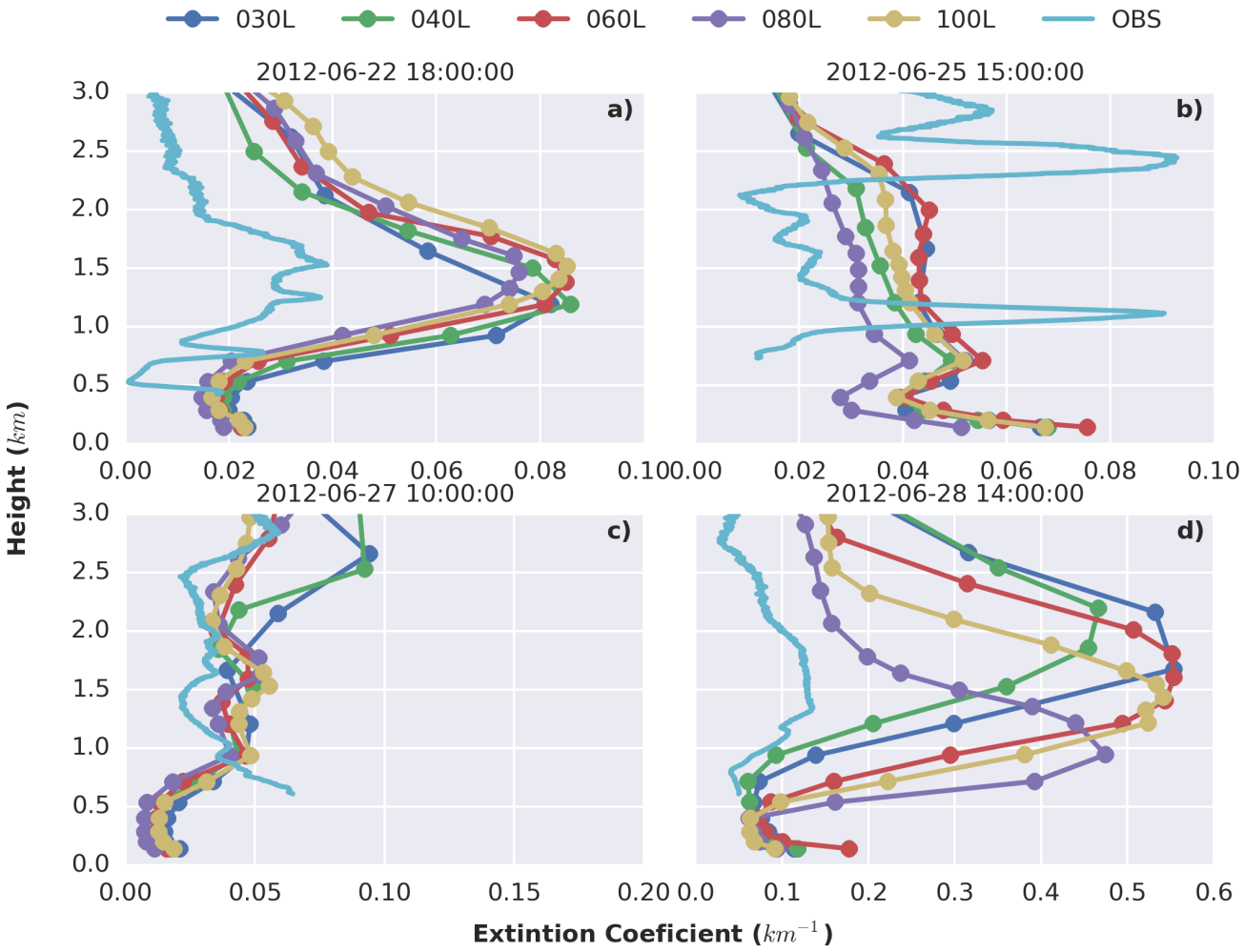

Figure 4: Vertical profiles of extinction coefficient (km^{-1}) at 532 nm at Barcelona for a) 22nd of June at 1800 UTC, b) 25th of June at 1500 UTC, c) 27th of June at 1000 UTC and d) 28th of June at 1400 UTC.